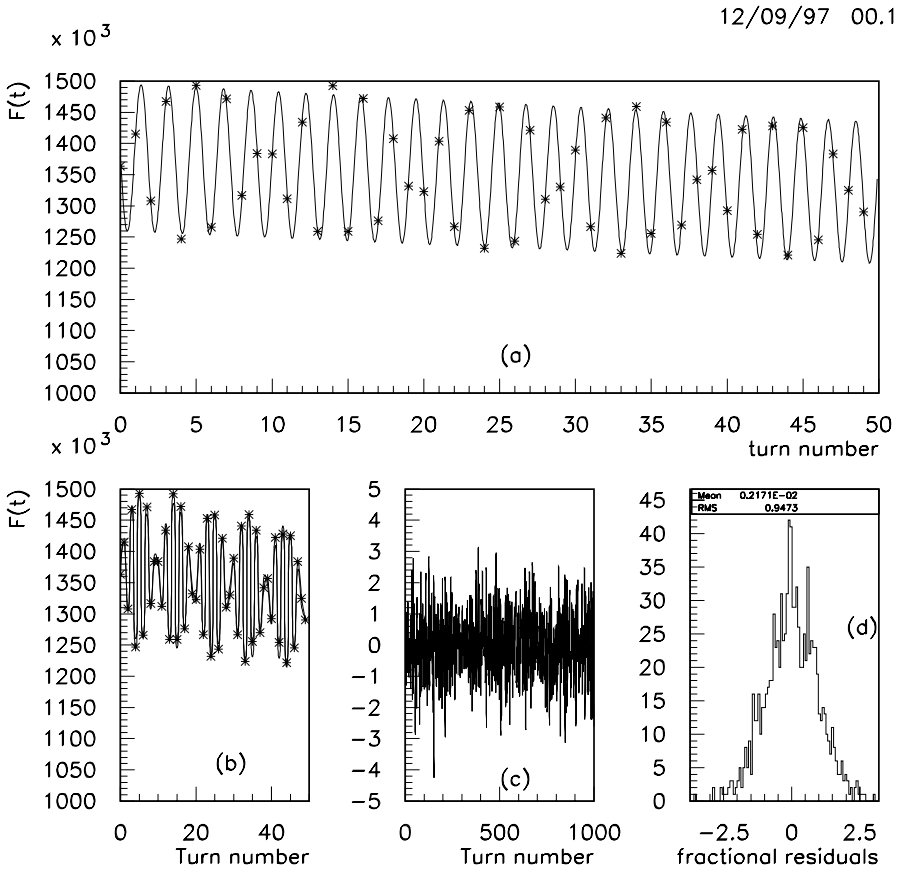


FIG. 58. a) Energy detected in the calorimeter during the first 50 turns in a 50 GeV muon storage ring (points). An average polarization value of $\hat{P} = -0.26$ is assumed and a fractional fluctuation of $5 \times 10^{-3}$ per point. The curve is the result of a MINUIT fit to the expected functional form. b) The same fit, with the function being plotted only at integer turn values. A beat is evident. c) Pulls as a function of turn number. d) Histogram of pulls. A pull is defined by (measured value-fitted value)/(error in measured-fitted).

sections in the collider ring. The length of the straight section upstream of the calorimeter can be chosen to control the total number of decays and hence the rate of energy deposition. The sensitive material can be gaseous, since the energy resolution is controlled by decay fluctuations rather than sampling error. In order to measure the total number of electrons entering the calorimeter, we plan to include a calorimeter layer with little absorber upstream of it as the first layer.

This scheme will enable us to calibrate and correct the energy of individual bunches of muons and permit us to measure the width of a low mass Higgs boson.

## VIII. RADIATION AND BACKGROUNDS

### A. Conventional radiation

The proton source generates a 4 MW proton beam, which is comparable to the proposed spallation source [92]. This is a very high power and will, as in the spallation source, require great care in reducing unwanted particle losses, as well as careful machine shielding, and target and beam dump design. Initial studies of the target and capture solenoid region have been performed with the MARS code, and preliminary specifications for shielding determined, but more work is needed.

The cooling and accelerator chain is rather clean, since a relatively small fraction of the muons decay, and their energies are low. Power deposited in the accelerators is typically 10-30 W/m (see table IX and table X).

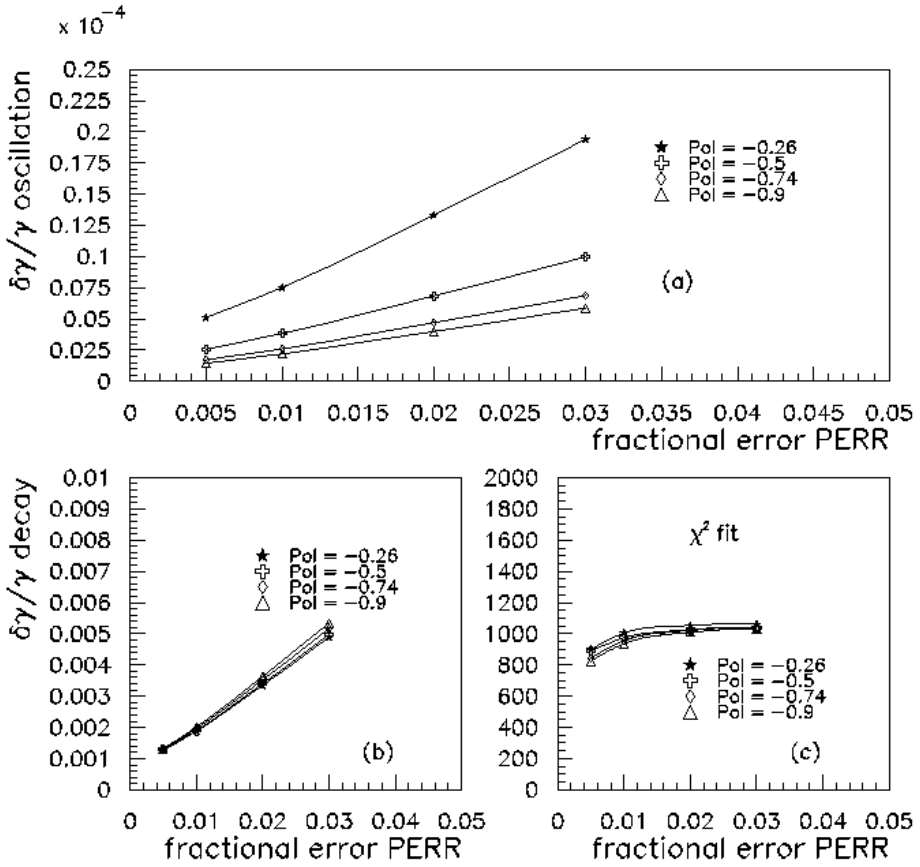


FIG. 59. a) Fractional error in $\delta\gamma/\gamma$ obtained from the oscillations as a function of polarization $\hat{P}$ and the fractional error in the measurements PERR. b) Fractional error in $\delta\gamma/\gamma$ obtained from the decay term as a function of polarization $\hat{P}$ and the fractional error in the measurements PERR. c) The total $\chi^2$ of the fits for 1000 degrees of freedom. PERR is the percentage measurement error on the total electron energy in the calorimeter measuring the decay electrons.

If no muons are lost, then the only sources of radiation are the muon decays yielding electrons and neutrinos. The neutrino radiation we discuss below. The electrons shower in the collider beam pipe shields, depositing most of their energy there and a relatively small amount in the magnet coils and yoke. Radioactivation levels, as calculated by MARS [215], after five years of 4 TeV collider operation are given in table XIV for the cases immediately after turn off and 1 day after turn off. It is seen that the areas in the tunnel that are outside the magnets are relatively free of radioactivation. Special procedures will be needed when the shield pipe has to be opened, as for instance when a magnet is changed. For the lower energy colliders, the radioactivation levels are proportionally less.

TABLE XIV. 4 TeV (CoM) collider ring radioactivation levels (mrem/hour) after turn off, for parameters in table I

| | immediate | after 1 day |
|---|---|---|
| Inside face of shield | 9000 | 4000 |
| Outside face of shield | 200 | 170 |
| Outside of coils | 30 | 14 |
| Outside of yoke | 3 | 1.4 |

If muons are lost either accidentally, by scraping, or deliberately after some number of turns, then the muons penetrate to considerable distances in the soil/rock (3.5 km at 2 TeV, 800 m at 250 GeV) and deposit their energy directly or through their interaction products. Figure 60 and Fig. 61 show the distribution of radiation levels, assuming 25% of all muons (4 bunches of $2 \times 10^{12}$ at 15 Hz) are dumped into soil/rock with density 2.24 g/cm$^3$. The outer contours correspond to the federal limits, reached at maximum radii of 18 m (2 TeV) and 14.5 m (250 GeV). To

confine this radiation beneath the ground one can deflect the extracted beams down by 4.5 mrad at 2 TeV and about 10 mrad at $\leq$250 GeV. If any water were present in the soil/rock, then the first two meters around the tunnel and around the aborted beam axis would require insulation or drainage up to a distance of 2.5 km at 2 TeV or 550 m at 250 GeV.

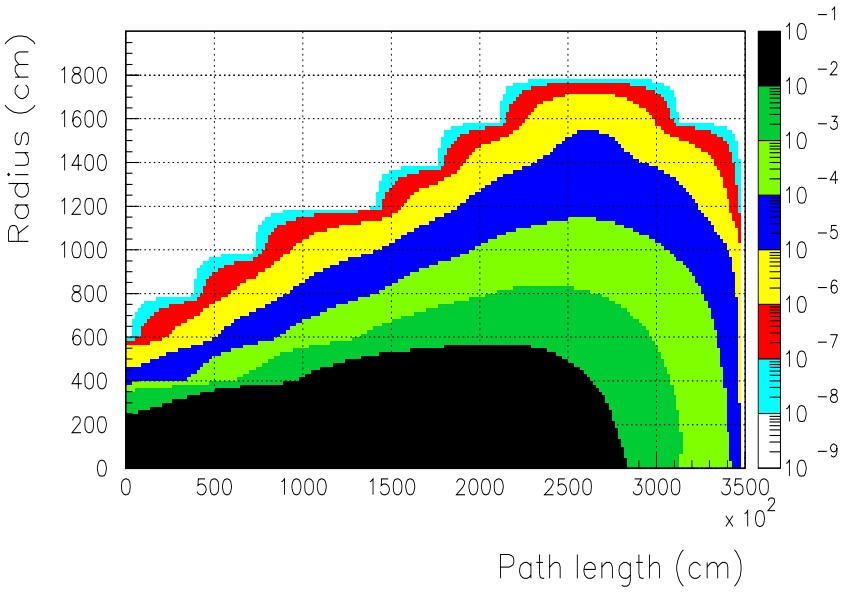


FIG. 60. Isodose contours in the soil/rock ($\rho$=2.24 g/cm$^3$) for 2 TeV muons extracted at $3 \times 10^{13}$ per second. Right scale is dose rate in rem/s.

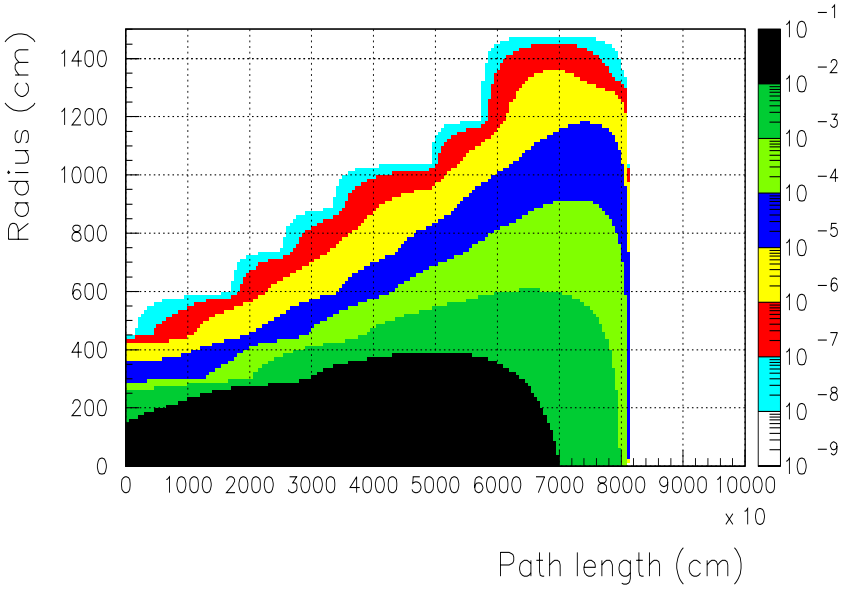


FIG. 61. Isodose contours in the soil/rock ($\rho$=2.24 g/cm$^3$) for 250 GeV muons extracted at $3 \times 10^{13}$ per second. Right scale is dose rate in rem/s.

### B. Neutrino induced radiation

It has been shown [64,216–219] that the neutrinos created in muon beam decays can generate excessive secondary radiation at large distances from a muon collider (see Fig. 62). The surface radiation dose $D_B(Sv)$ in units of equivalent [220] doses $(Sv)$ over a time $t(s)$, in the plane of a bending magnet of field B(T), in a circular collider with beam energy $E(TeV)$, average bending field $< B(T) >$, at a depth $d(m)$ (assuming a spherical earth), with muon current (of each sign) of $I_\mu$(muons/s/sign) is given by:

$$D_B \approx 4.4 \times 10^{-24} \frac{I_\mu E^3 t}{d} \frac{< B >}{B} \tag{31}$$

and the dose $D_S$ at a location on the surface, in line with a high beta straight section of length $\ell(m)$, is:

$$D_S \approx 6.7 \times 10^{-24} \frac{I_\mu E^3 t}{d} \ell < B >. \tag{32}$$

The equation for $D_S$ assumes that the average divergence angles satisfy the condition: $\sigma_\theta << \frac{1}{\gamma}$. This condition is not satisfied in the straight sections approaching the IP, and these regions, despite their length, do not contribute a significant dose.

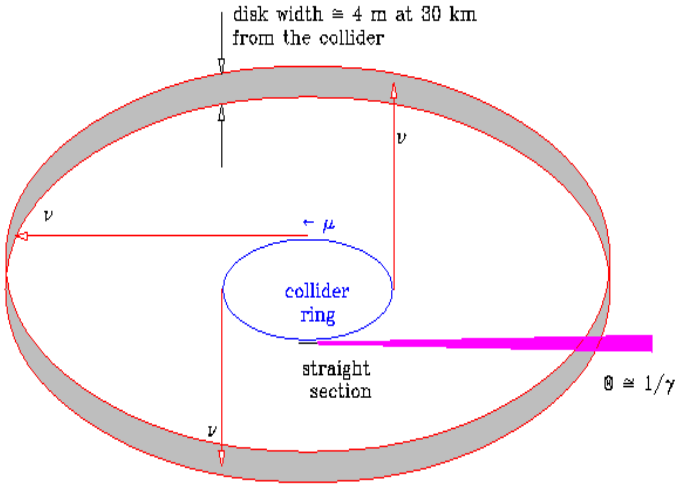


FIG. 62. Neutrino radiation disk. For a 3 TeV CoM collider the neutrino radiation width is ≈ 4 m at a distance of 30 km. A *hot spot* produced by 0.1 m straight section in the ring contains roughly twice the number of neutrinos on the disk on average, depending on the details of the collider lattice.

For the 3 TeV parameters given in table I and muon currents $I_\mu = 6 \times 10^{20}\, \mu^-/yr$, $< B >= 6\ T$, $B = 10\ T$ and depth = 500 m, and taking the Federal limit on off-site radiation dose/year, $D_{\rm Fed}$, to be 1 mSv/year (100 mrem/year), the annual dose $D_B$ (1 year is defined as $10^7$ s), in the plane of a bending dipole is,

$$D_B = 1.07 \times 10^{-5}\ \text{Sv} \approx 1\%\ D_{\rm Fed}, \tag{33}$$

and for a straight section of length 0.6 m is:

$$D_S = 9.7 \times 10^{-5}\ \text{Sv} \approx 10\%\ D_{\rm Fed}, \tag{34}$$

which may be taken to be within a reasonable limit. The general trend of these expressions has been verified by Monte Carlo simulations [221] using MARS. In particular, for the 3 TeV case the needed depth to stay within 1% $D_{\rm Fed}$, is 300 m instead of 500 m.

Special care will be required in the lattice design to assure that no field- free region longer than 0.6 m is present. This may sound difficult, but it may be noted that the presence of a field of even 1 T, is enough to reduce the dose to a level below the Federal limit. The application of such a field over all rf and other components seems possible [221].

For lower energy machines, the requirements rapidly get easier: a 0.5 TeV machine at 100 m depth could have 25 m long sections, for the same surface dose. For a 100 GeV machine the doses are negligible.

For machines above 3 TeV, various strategies can be employed:

- The machines could be built at greater depths (mines many km deep are common).
- The vertical beam orbits in the machine could be varied so as to spread the plane of radiation and thus reduce the peak doses.
- The specific locations in line with straight sections could be purchased and restricted.
- Straight sections could be shortened further by using continuous combined function magnets.
- The machines could be built on an island, but this could have difficulties associated with access to power and other utilities.

But for any large increase in energy, to 10 TeV for instance, some reduction in muon beam flux probably will be required. The resultant loss of luminosity might be made up in a number of ways [4]:

- The beam-beam tune shift constraint could be avoided by introducing a conducting medium (e.g. liquid lithium) at the interaction point [222].
- The focusing strength could be increased by the use of plasma or other exotic focusing method.
- Better cooling could be developed. Optical stochastic cooling [139], for instance, might reduce the emittances by many orders of magnitude, thus greatly reducing the required beam currents. Indeed, such cooling would require lower currents to function appropriately.

Such options will need future study.

### C. Muon decay background

With $4 \times 10^{12}$ muons per bunch in a 2 + 2 TeV collider ring there are approximately $4 \times 10^5$ muon decays per meter giving rise to high energy electrons. These off-energy, off-axis electrons undergo bremsstrahlung when they traverse magnetic fields. When they exit the beam pipe they interact and produce electromagnetic showers and, to a lesser extent, hadrons and muons. Much of this debris can be locally shielded, so the primary concern is muon decays near the interaction point [44]. This is the background we discuss in some detail below.

Detailed Monte Carlo simulations of electromagnetic, hadronic and muon components of the background [44,195,206,211,221,223,224] have been performed using the MARS [115] and GEANT [151] codes. The most recent study [223] has been done with GEANT. Figure 63 shows the final 130 meters of the 2 + 2 TeV detector region in this study. It includes the final four quadrupoles, dipoles and a solenoidal field surrounding the detector. This study:

- followed shower neutrons and photons down to 40 keV and electrons to 25 keV.
- used a tungsten shield over the beam, extending outward to an angle of 20 degrees from the axis.
- Inside this shield, the clear radius has a minimum, in the high energy cases, at a distance from the IP of 1.1 m (80 cm for 50+50 GeV). At this point, and in an expanding cone beyond it, the clear radius is maintained at approximately 4 sigma of the beam size.
- Between this minimum aperture point and the IP, the clear radius follows an inverse cone, increasing as it approaches the IP, with an angle a little greater than the 4 sigma of the beam divergence. These cones are designed so that the detector could not 'see' any surface directly illuminated by the initial decay electrons, whether in the forward or backward (albedo) direction (see figure 64).
- The resulting open space between the IP and the tip of the cone is approximately 3 cm in the 4 TeV and 500 GeV CoM cases, and approximately 6 cm in the 100 GeV CoM case.
- The inner surface of each shield is shaped into a series of collimating steps and slopes to maximize the absorption of electron showers from electrons at very small angles to the cone surface, thus reducing the funnelling of low energy electrons down the pipes.
- Further upstream, prior to the first quadrupole (from 2.5 to 4 m in the Higgs case), an 8 T dipole, with collimators inside, is used to sweep decay electrons before the final collimation.

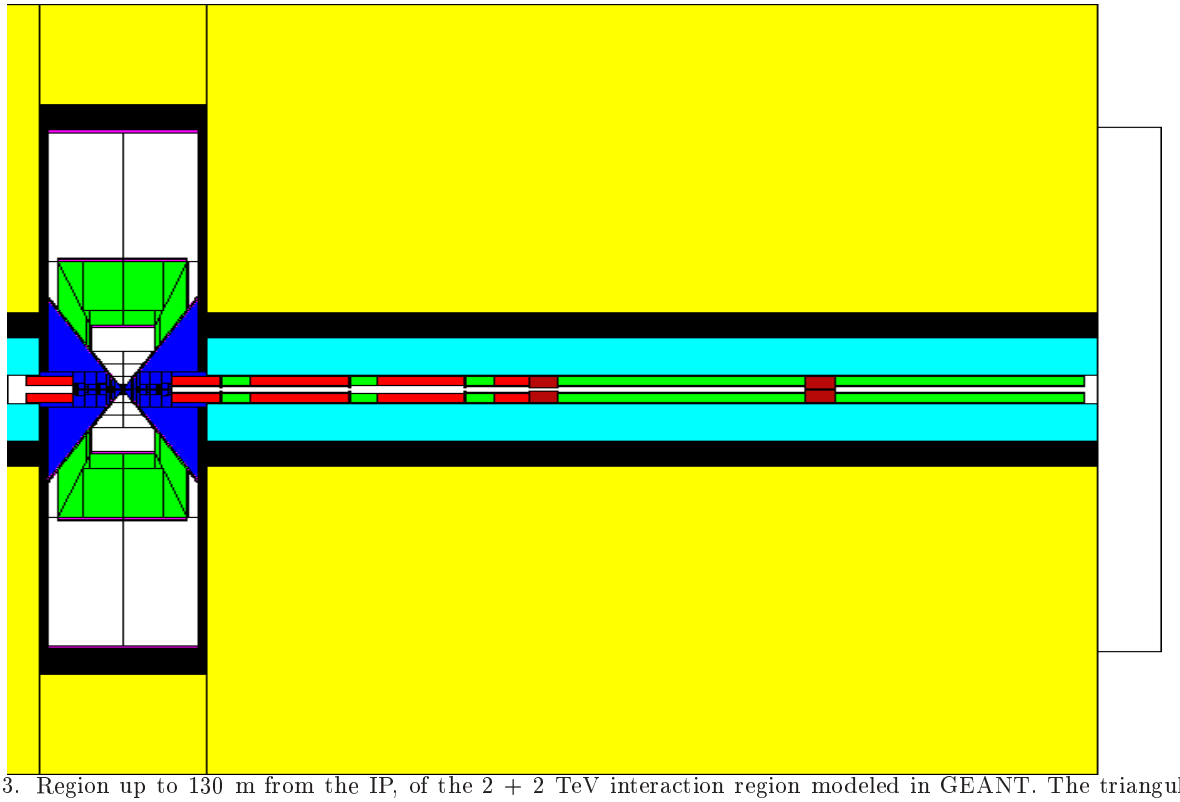

FIG. 63. Region up to 130 m from the IP, of the 2 + 2 TeV interaction region modeled in GEANT. The triangular blue regions represent tungsten shielding. On the right hand of the figure, the red areas represent quadrupoles in the beam line. The areas around the IP represent the various detector volumes used in the calculations of particle fluences. The detector (white and green areas) is 10 m in diameter and 20 m long.

Note that there is currently an inconsistency, in the very low $\Delta p/p$ Higgs Factory Case, between the short open space between shields (+/- 6 cm) and the rms source length ($\sigma_{\rm source} = 1/\sqrt{(2)}\sigma_z$) of 10 cm. Some modifications to the parameters and shielding design will be required for this case.

Every modern detector will have to be able to identify and reconstruct secondary vertices such as those associated with b-quark decays. In order to estimate the viability of a vertex detector we have to show that the occupancy of its elements is not higher than about 1%. Figure 65 shows the occupancy as a function of radial distance from the interaction point for the three CoM energies studied : 0.1, 0.5 and 4 TeV. The occupancy was calculated for silicon pads of 300 $\mu m \times 300$ $\mu m$, and assuming interaction probabilities of 0.003 and 0.0003 for low energy photons and neutrons respectively. One can observe that the total occupancy (left figure) is above one percent for small radii. Most of the hits is due to conversions of photons. The occupancy due to hits resulting from charged particles is below 1% (right hand figure). One can lower the occupancy at small radii by using smaller pixel sizes, as indicated in table XV below, as well as by using innovative detector ideas as described in the next section.

Table XV gives the hit density for the Higgs factory from the various sources and the occupancy of pixels of the given sizes; in each case the number is given per bunch crossing. The hit density for the higher energy machines is found to be somewhat lower due to the smaller decay angles of the electrons.

TABLE XV. Detector backgrounds from $\mu$ decay

| Radius | $cm$ | 5 | 10 | 20 | 100 |
|---|---|---|---|---|---|
| Photons hits | $cm^{-2}$ | 26 | 6.6 | 1.6 | 0.06 |
| Neutrons hits | $cm^{-2}$ | 0.06 | 0.08 | 0.2 | 0.04 |
| Charged hits | $cm^{-2}$ | 8 | 1.2 | 0.2 | 0.01 |
| Total hits | $cm^{-2}$ | 34 | 8 | 2 | 0.12 |
| Pixel size | $\mu m \times \mu m$ | 60 × 150 | 60 × 150 | 300 × 300 | 300 × 300 |
| Total occupancy | % | 0.6 | 0.14 | 0.4 | 0.02 |
| Occupancy charged | % | 0.14 | 0.02 | 0.04 | 0.002 |

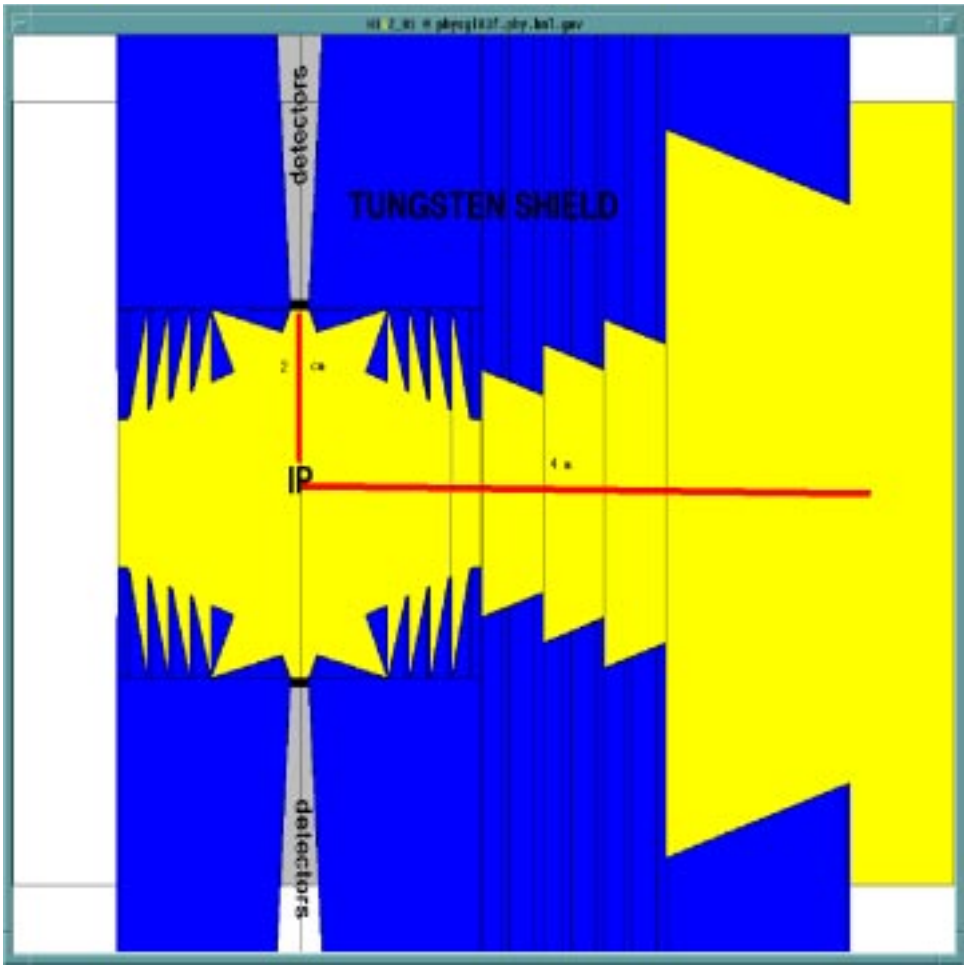


FIG. 64. Detail of the tungsten shielding designed for the 50 + 50 GeV case. It is designed so that the detector is not connected by a straight line with any surface hit by decay electrons in forward or backward directions. The picture extends out to a radius of 6 cm and, on the right, to a distance 4 m from the IP. The dipole from 2.5-4.0 m is not shown.

The radiation damage by the neutrons on a silicon detector has also been estimated. In the Higgs case, at 5 cm from the vertex, the number of hits from neutrons above 100 keV is found to be $1.8 \times 10^{13}/\mathrm{cm}^2$ per year. This is significantly less than that expected at the LHC which is now ordering silicon detectors claimed to survive $5 \times 10^{14}$ hits, approximately three times that assumed here. The damage for silicon detectors in the higher energy machines is of the same order (see table XVI).

TABLE XVI. Radiation damage by neutrons on silicon detectors. The working assumptions are: 1000 turns, 15 Hz and 1 year=$10^7$ s. An acceptable number of hits per year is $1.5 \times 10^{14}$.

| CoM (TeV) | $\mu$'s/bunch ($10^{12}$) | neutrons/cm$^2$/crossing (above 100 KeV) | Hits/cm$^2$/year ($10^{13}$) | Lifetime (years) |
|---|---|---|---|---|
| 4 | 2 | 100 | 3 | 5 |
| 0.5 | 4 | 50 | 3 | 5 |
| 0.1 | 4 | 30 | 1.8 | 8 |

### D. Halo background

Muon halo refers to those muons which are lost from the beam bunch as it circulates around the collider ring. In conventional electron or proton accelerators, beam particles which are lost away from the IP are of little concern as

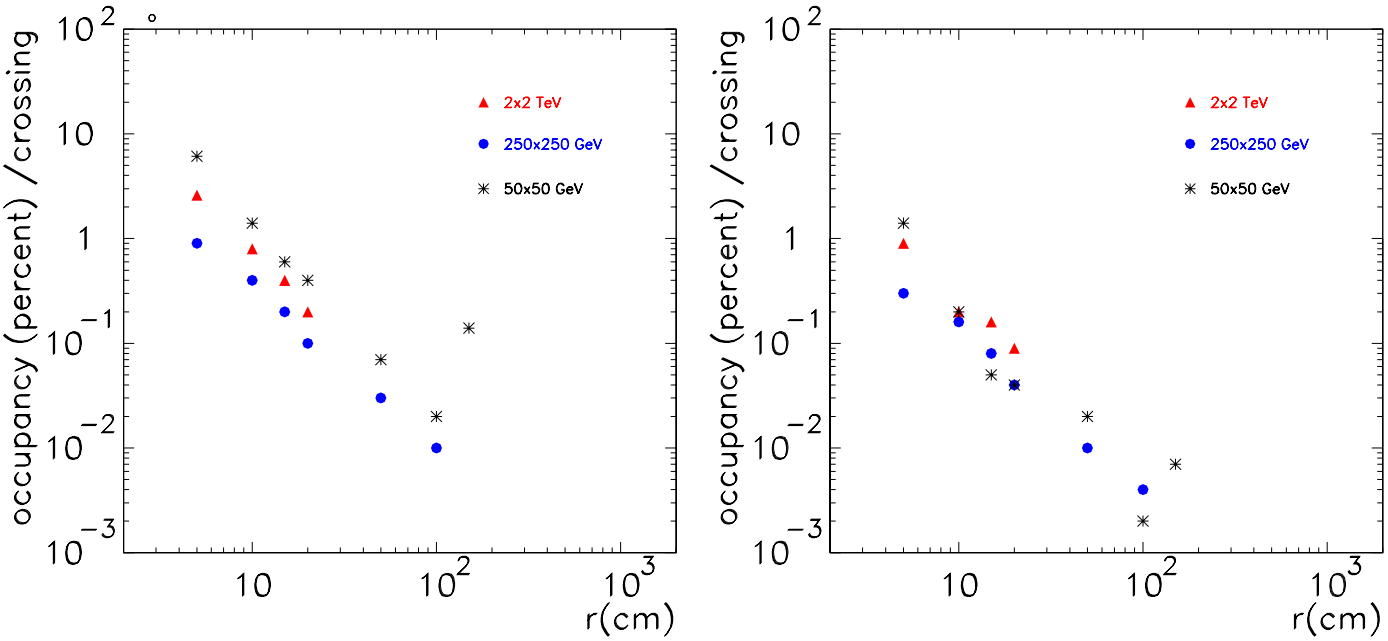


FIG. 65. Occupancy for 300 $\mu\,m \times 300\ \mu\,m$ silicon pads, as a function of the radius for the three energies studied. Left figure shows the total occupancy and the right figure shows the occupancy from hits resulting from charged particles.

they can be locally shielded. However, muons can traverse long distances and therefore have the potential to generate background in a detector. The magnitude of this background depends on a detailed knowledge of the injected beam profile and a credible model for beam halo and beam losses. More work is needed before these are well enough understood. Nevertheless, it is clear that the beam will need careful preparation before injection into the collider, and the injection system will have to be precise and free of ripple.

The collimation system described in the previous subsection was designed to scrape the beam both initially and during the 1000 turns, to assure that all loss occurs at the scraper and not near the IP. That study indicated suppressions better than $10^3$ of background in the detector [196].

Beam loss must be limited as far as possible. Gas scattering has been studied [225] and shown to give a negligible contribution. The effects of beam-beam scattering are under study and need further work. Momentum spread tails from uncorrected wakefield effects must be controlled. Assuming that the total loss from all causes, after injection and the first few turns is less than $10^{-4}$ in 1000 turns, (i.e. $10^{-7}$ per turn), then the number of background muons passing through the detector should be less than 800 ($2 \times 4 \times 10^{12} \times 10^{-7} \times 10^{-3}$) per turn. This is a low density of tracks per cm$^2$ and should be acceptable, but lower losses or better scraping would be desirable.

### E. Pair production

Coherent beam-beam electron pair production (beamstrahlung) has been shown [208,226] to be negligible, but the incoherent pair production (i.e. $\mu^+\mu^- \rightarrow \mu^+\mu^- e^+ e^-$) in the 4 TeV collider case is significant.

The cross section is estimated to be 10 mb [226], which would give rise to a background of $\approx 3 \times 10^4$ electron pairs per bunch crossing. The electrons at production do not have significant transverse momentum but the fields of the on-coming 3$\mu$m bunch can deflect them towards the detector. A simple program was written to track electrons from

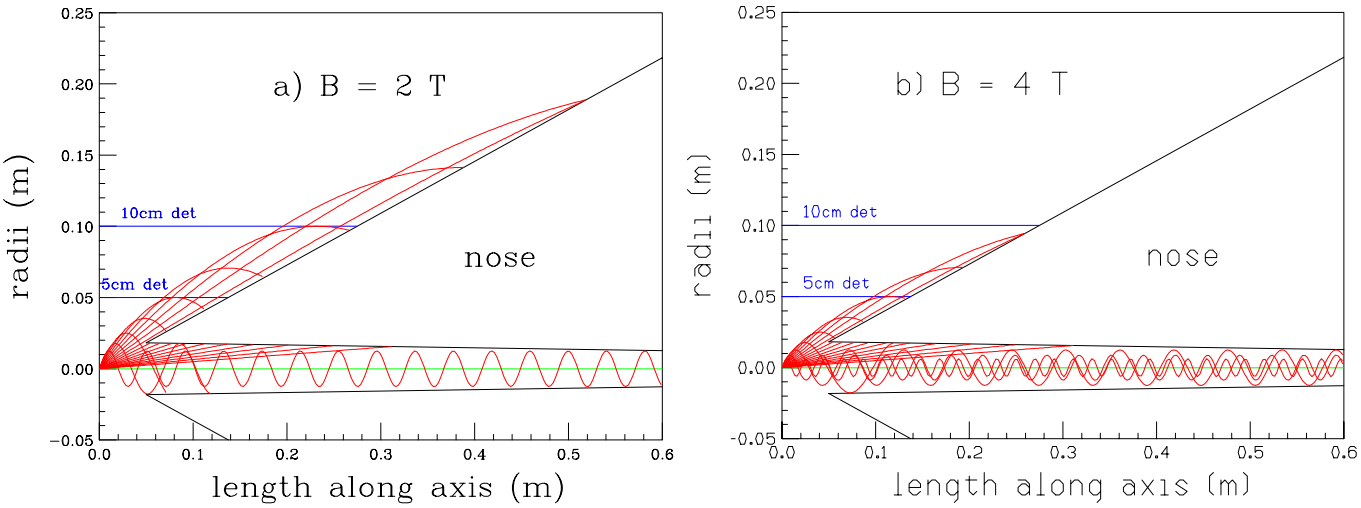


FIG. 66. Radius vs. length of electron pair tracks for initial momenta from 3.8 to 3000 MeV in geometric steps of $\sqrt{2}$; (a) for a solenoid field of 2 T, (b) for 4 T.

close to the axis (the worst case) as they are deflected away from the bunch center. Once clear of the opposing bunch the tracks spiral under the influence of the experimental solenoid field. Figures 66 shows the radii vs. length of these electron tracks for initial momenta from 3.8 to 3000 MeV in geometric steps of $\sqrt{2}$. Fig. 66(a) is for a solenoidal field of 2 T and Fig. 66(b) for 4 T. In the 2 T case tracks with initial energy below 30 MeV do not make it out to a detector at 10 cm, while those above 100 MeV have too small an initial angle and remain within the shield. Approximately 10% (3000 tracks) of these are in this energy range and pass through a detector at 10 cm. The track fluences at the ends of the detector are less than 10 tracks per cm$^2$ which should not present a serious problem. At 5 cm, there are 4500 tracks giving a fluence of 30 per cm$^2$, which is also probably acceptable. If the detector solenoid field is raised to 4 T, then no electrons reach 10 cm and the flux at 5 cm is reduced by a factor of 2.

### F. Bethe-Heitler muons

TABLE XVII. Bethe-Heitler Muons

| CoM Collider Energy (TeV) | 4 | 0.5 | 0.1 |
|---|---|---|---|
| Assumed source length (m) | 130 | 33 | 20 |
| $\mu$ ($p_{muon} > 1$ GeV/$c$) per electron | $5.4 \times 10^{-4}$ | $8.3 \times 10^{-5}$ | $9.6 \times 10^{-6}$ |
| Beam $\mu$'s per bunch | $2 \times 10^{12}$ | $2 \times 10^{12}$ | $4 \times 10^{12}$ |
| Bethe-Heitler $\mu$'s per bunch crossing ($\times 10^3$) | 28 | 17.5 | 6.1 |
| $< p_{muon} >$ initial (GeV) | 22 | 9.5 | 4.4 |
| $\mu$'s entering calorimeter | 220 | 160 | 25 |
| $< p_{muon} >$ (GeV) | 15.4 | 6.3 | 1.8 |
| $< E_{dep} >$ (GeV) | 2.9 | 1.3 | 0.4 |
| Total $E_{dep}$ (GeV) | 640 | 210 | 10 |
| $E_{dep}$ pedestal subtracted (GeV) | 50 | 25 | 1 |
| Fluctuation in $E_{dep}$ (GeV) | 55 | 15 | 1 |
| $E_{trans}$ pedestal subtracted (GeV) | 15 | 15 | .5 |
| Fluctuation in $E_{trans}$ (GeV) | 40 | 8 | 0.5 |

The GEANT/MARS studies [44,211,215] also found a significant flux of muons with quite high energies, from $\mu$ pair production in electromagnetic showers (Bethe-Heitler). Figures 67 and 68 show the trajectories of typical muons from their sources in the shielding around the beam pipe to the detector. Figure 67 is for a 4 TeV CoM collider, where the muons have high energy and long path lengths. A relatively long (130 m) section of beam pipe prior to the detector is shown. Figure 68 is for the 100 GeV CoM collider for which, since the muons have rather short path

lengths, only a limited length of beam pipe is shown. Note that the scales are extremely distorted: the $20^o$ shielding cones on the right hand of the figures appear at steeper angles.

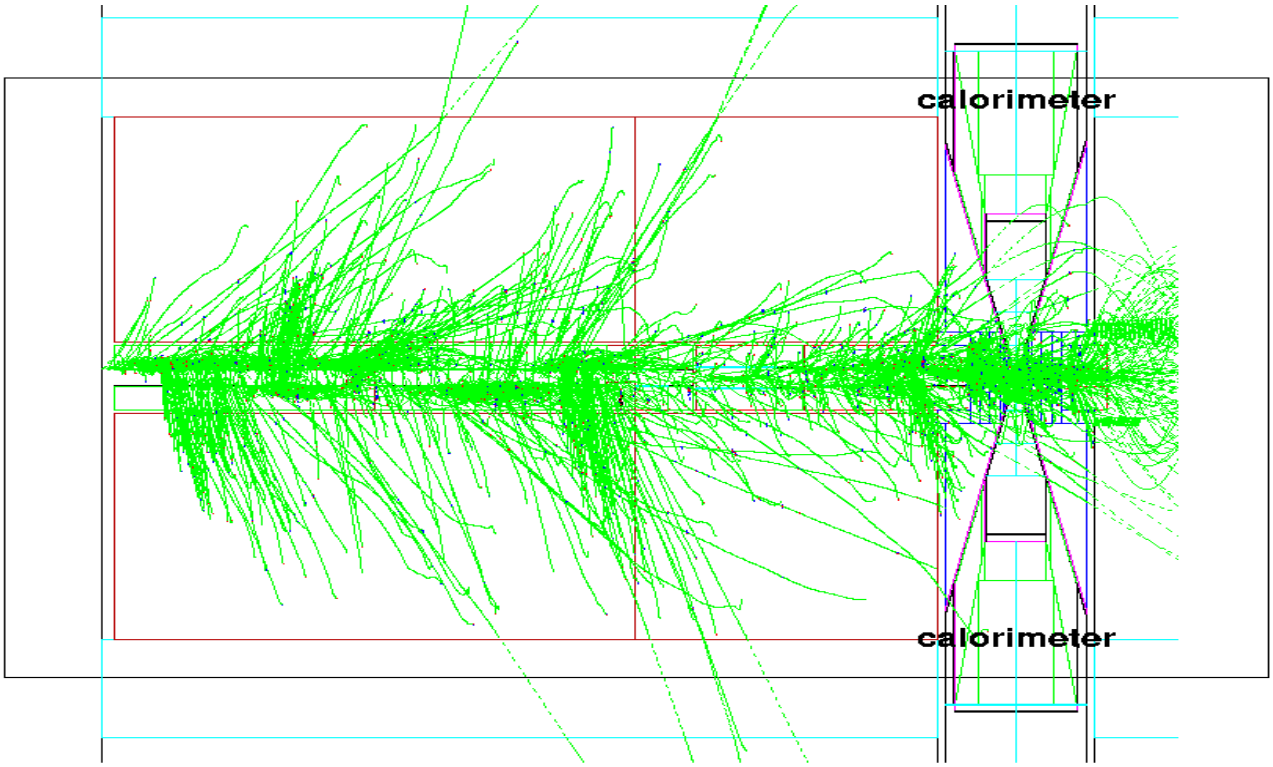


FIG. 67. Trajectories of typical Bethe-Heitler muons from their source in the shielding around the beam pipe to the detector for a 4 TeV CoM collider. As indicated in the text the scales are extremely distorted, the total horizontal length is $\approx$ 130 m and the outer edge of the calorimeter is $\approx$ 4 m. Notice that $< 1\%$ of the tracks end in the calorimeter (see table XVII).

The most serious effect appears to arise when these muons make deeply inelastic interactions and deposit spikes of energy in the electromagnetic and hadronic calorimeters. This is not serious in the Higgs case, for which the fluxes and cross sections are low, but at the higher collider energies they generate significant fluctuations in global parameters, such as transverse energy and missing transverse energy.

Table XVII gives some parameters of the muons for three different machine energies. In the 4 TeV and 500 GeV CoM cases, massive lead shielding outside the focus quadrupoles has been included.

Figures 69 and 70 show energy deposition from Bethe-Heitler muons in a typical bunch crossing. These depositions are plotted against the cosine of the polar angle and azimuthal angle in the calorimeter for 4 TeV and for 500 GeV CoM, respectively. The massive lead shielding referred to above was not included in this study. Right hand plots in Figs. 69 and 70 show the same distributions with a 1 ns timing cut. It is seen that the timing cut, if it is possible, is effective in removing energy spikes at small rapidity, but has little effect in the forward and backward directions. The overall reduction in energy deposition is about a factor of two.

The energy spikes can cause at least three problems: 1) they affect the triggers and event selections based on overall or transverse energy balance; 2) they can generate false jets and 3) they can give errors in the energies of real jets. After a pedestal subtraction, the effects on energy balances do not seem serious. The generation of false jets can be eliminated by a longitudinal energy distribution cut without introducing significant inefficiency. Energy errors in real jets appear to be the most serious problem. They can be reduced by the application of radial energy distribution cuts, but such cuts introduce significant inefficiencies for lower energy jets. More study is needed.

Earlier studies [224] with MARS, using less sophisticated shielding, gave results qualitatively in agreement with those from GEANT.

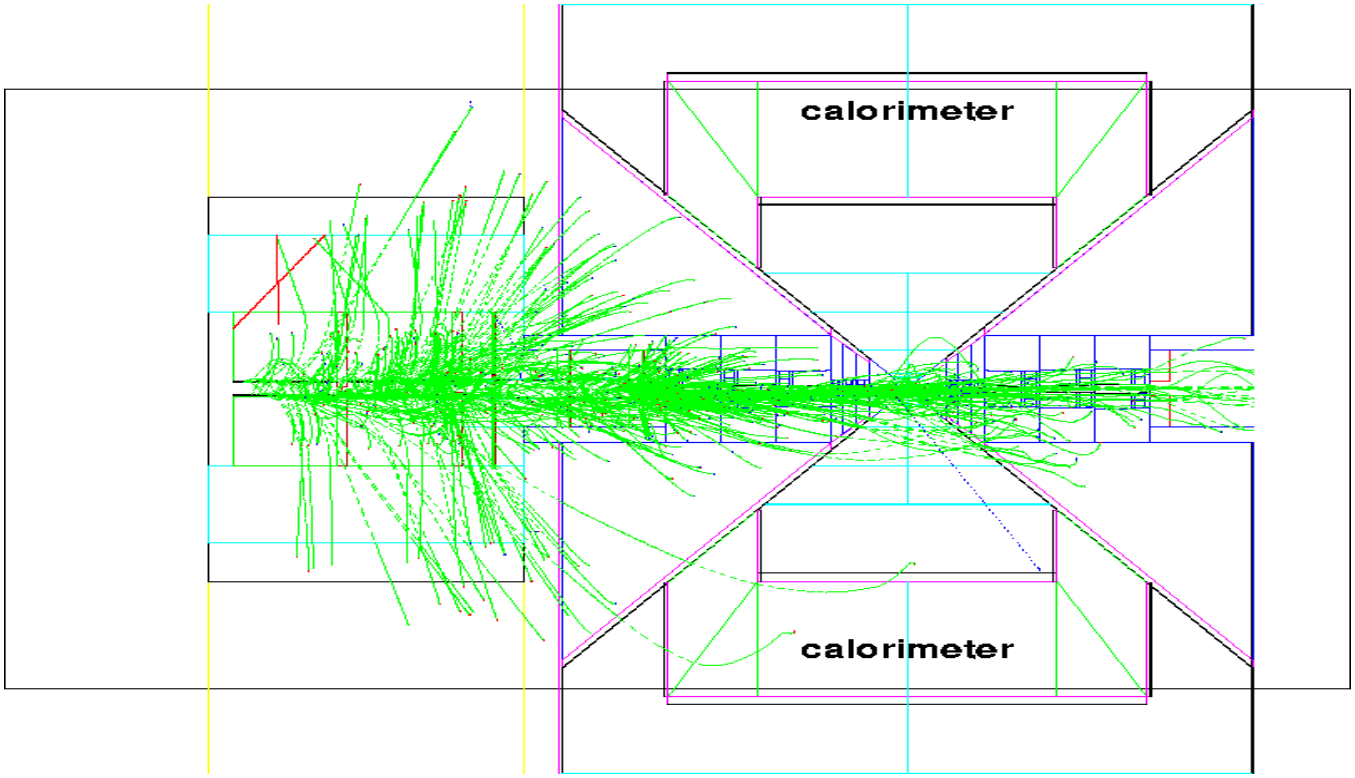


FIG. 68. Trajectories of typical Bethe-Heitler muons from their source in the shielding around the beam pipe to the detector for a 100 GeV CoM collider. As indicated in the text the scale is extremely distorted, the total horizontal length is $\approx$ 20 m and the outer edge of the calorimeter is $\approx$ 4 m. Notice that $< 0.5\%$ of the tracks end in the calorimeter (see table XVII).

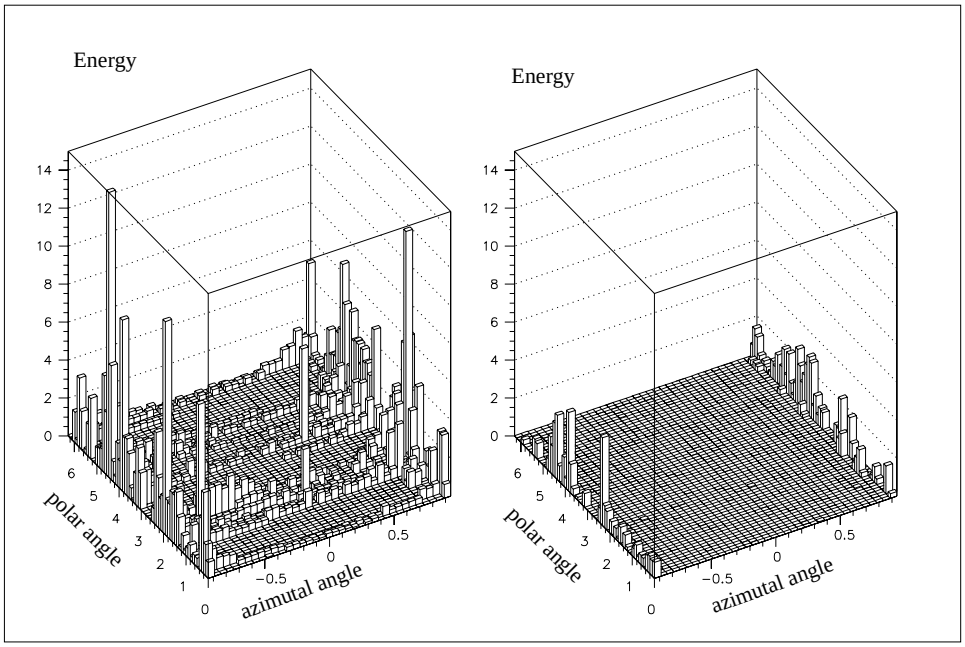


FIG. 69. Left hand plot shows the energy deposition from Bethe-Heitler muons *vs.* the cosine of the polar angle and azimuthal angle in the calorimeter for a 4 TeV CoM collider. Right hand plot shows the same distributions with a 1 ns timing cut.